# Snowflake Divertor Studies in DIII-D and NSTX Aimed at the Power Exhaust Solution for the Tokamak

V. A. Soukhanovskii[1], S. L. Allen[1], E. Kolemen[2], T. H. Osborne[3], J. A. Boedo[4], M. E. Fenstermacher[1], R. J. Groebner[3], D. N. Hill[1], A. W. Hyatt[3], C. J. Lasnier[1], A. W. Leonard[3], M. A. Makowski[1], W. H. Meyer[1], A. McLean[1], T. W. Petrie[3], D. D. Ryutov[1], J. G. Watkins[5], R. E. Bell[2], A. Diallo[2], S. P. Gerhardt[2], R. Kaita[2], S. Kaye[2], B. P. LeBlanc[2], R. Maingi[2], J. E. Menard[2], M. Podesta[2], R. Raman[6], A. L. Roquemore[2], F. Scotti[2]

[1]*Lawrence Livermore National Laboratory, Livermore, CA, USA*
[2]*Princeton Plasma Physics Laboratory, Princeton, NJ, USA*
[3]*General Atomics, San Diego, CA, USA*
[4]*University of California at San Diego, La Jolla, CA, USA*
[5]*Sandia National Laboratories, Livermore, CA, USA*
[6]*University of Washington, Seattle, WA, USA*

**Introduction** A snowflake divertor (SF) configuration [1] is a promising concept for the tokamak divertor power exhaust problem, with increasing experimental support from TCV [2, 3], NSTX [4, 5, 6] and DIII-D tokamaks [7]. The SF magnetic configuration uses a second-order null-point created by bringing two first-order null-points of the standard divertor together [1, 8, 9, 10, 11]. Poloidal magnetic flux surfaces in the region of the exact second-order null have six hexagonal separatrix branches with an appearance of a snowflake. The exact second-order null configuration is topologically unstable [1], therefore, in experiments, two variants of the exact configuration called snowflake-plus and snowflake-minus [8, 9] are often realized in steady-state. The broadened low $B_p$ region surrounding the null(s) (e.g., as shown in Figure 1) has a strong impact on divertor power balance, heat transport and heat deposition on plasma-facing components, via increased divertor plasma-wetted area, additional divertor legs (strike points), increased X-point-to-target connection length and divertor volume [1]. A high $\beta_p$ region that forms in the SF divertor can also lead to the onset of fast convective heat transport and as a result, increased power sharing between separatrix branches (divertor legs) [10, 11, 12]. Additional insights into the SF divertor physics are being provided by high divertor power-density experiments conducted in NSTX and recently, at DIII-D. Both tokamaks have open divertors with graphite plasma-facing components and divertor heat fluxes of several MW/m$^2$. In both tokamaks, greatly reduced divertor heat fluxes between and during ELMs were measured in the SF configuration, compatible with high performance H-mode operation (H98y2>1). In this paper we discuss NSTX and DIII-D results in the context of further SF concept development for future devices, namely, with respect to compatibility with radiative divertor and detachment, and compatibility with cryo-pump density control.

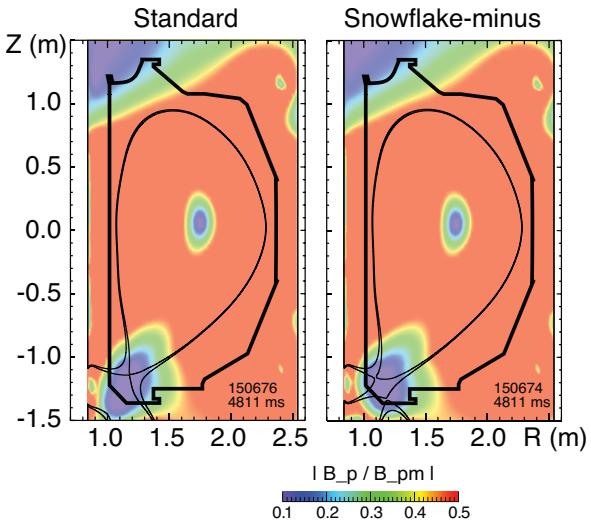


***Figure 1:*** *Plasma equilibria and poloidal field modulus normalized to its outer midplane value $|B_p/B_{pm}|$ in DIII-D discharges with the standard divertor; SF-minus configurations.*

**Divertor geometry** In both tokamaks, significant geometry benefits were realized in the SF-minus configuration. SF configurations was produced using three standard poloidal field shap-

| | Minor radius $a$ (m) | $P_{NBI}$ (MW) | $I_p$ (MA) | $\lambda_q$ (mm) | $f_{exp}$ Standard / SF | $L_{\|\|}$ Standard / SF | $D$ (m) |
|---|---|---|---|---|---|---|---|
| NSTX | 0.58 | 4 | 0.9 | 5 | 10-20 / 30-80 | 10-12 / 15-60 | 0.125 |
| DIII-D | 0.60 | 5 | 1.2 | 2.5-3 | 10 / 30-40 | 50 / 50-150 | 0.1 |

***Table 1:*** NSTX and DIII-D parameters in the SF divertor experiments described in this paper.

ing coils in the divertor region. The plasma control systems in both tokamaks are similar, and they were configured to run with pre-programmed divertor coil currents using an algorithm described in [5]. While in both NSTX and DIII-D, the exact SF and the SF-plus configurations were obtained for shorter periods of time, the use of the algorithm enabled only the SF-minus to be sustained for periods comparable with discharge duration (e.g., Figure 1). In both tokamak experiments, the ion $\nabla B$ direction was toward the lower divertor. Due to the poloidal field $B_p$ structure in the SF [10, 11], the geometry benefits for the SOL heat flux channel realized in the SF-minus are similar to those of the exact SF configuration when the distance $D$ between nulls satisfies $D \leq a\,(\lambda_q/a)^{1/3}$ (where $a$ is the minor radius and $\lambda_q$ is the SOL power width (projected to midplane)). The appropriate parameters from the NSTX and DIII-D experiments are summarized in Table 1. Between-null distance $D$ obtained in the experiments is within 50 % of the estimated, and indeed, a significant increase (cf. standard divertor) in the plasma-wetted area (poloidal flux expansion $f_{exp}$), connection lengths $L_{||}$, and divertor volume have been obtained in both NSTX [4, 5] and DIII-D [7]. Shown in Figure 2 are time traces and divertor profiles of two DIII-D H-mode discharges with the standard and the SF-minus divertor and the same density $n_e/n_G \simeq 0.45$ (where $n_G$ is the Greenwald density). The divertor radiated power remained similar in both discharges, as was the confinement, whereas the peak heat flux was reduced by 50-60 % in the SF-minus discharge. Divertor profiles show that heat flux was significantly reduced in the zone affected by very low $B_p$, and apparently, the reduction was mostly due to the flux expansion. The extent of the zone and its effect on $f_{exp}$ and $L_{||}$ radial profiles are dependent on the location of the secondary null. In NSTX, the second-null location projected to the mid plane radius was at 1-4 mm normalized flux surface (cf. $\lambda_q = 5-6$ mm), whereas in DIII-D it was between 1 and 4 mm flux surface (cf. $\lambda_q = 2.5-3$ mm [13]), thereby significantly affecting the steady-state SOL heat flow channel in both cases. In future devices, where the SOL width scaling $\lambda_q \sim a/I_p$ is expected [13], the required distance between nulls $D$ may be small and will have to be controlled via the plasma control system. This capability is presently being developed for DIII-D and NSTX-U [14].

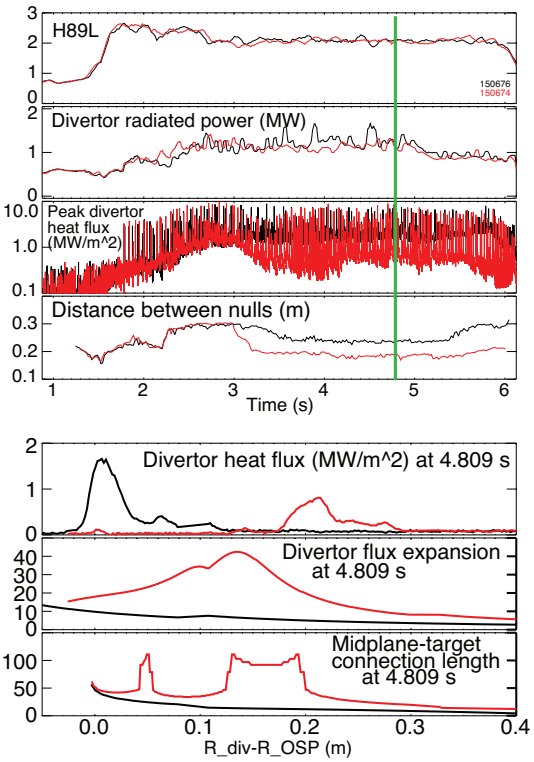


***Figure 2:*** *Comparison of DIII-D H-mode discharges with the standard divertor (black time traces) and SF-minus (red traces, top panel). Bottom panel, same color notation: divertor profiles measured in both discharges at 4.8 s.*

**Detachment** The SF geometry could lead to a facilitated access to the outer strike point (OSP) detachment. Increased volumetric power and ion momentum losses could reduce $q_{||}$, while a higher divertor $f_{exp}$ could lead to a higher degree of "plasma plugging" for recycling neutrals and reduce divertor $T_e$, thereby further increasing volumetric losses. Results obtained

in the SF-minus configurations differed in NSTX and DIII-D w.r.t. detachment onset.

In NSTX, the SF-minus formation was always accompanied by a stable partial detachment of the OSP. In the NSTX standard divertor configuration, partial detachment was inaccessible at $P_{SOL} = 3$ MW and $n_e/n_G = 0.6 - 0.8$ unless additional divertor gas puffing was used [15]. In the SF-minus, the between-ELM peak heat flux $q_{peak}$ was reduced from 3-7 MW/m$^2$ to 0.5-1 MW/m$^2$. As the SF configuration was formed, the $q_{peak}$ reduction factor quickly exceeded the factor by which plasma-wetted area was increased ($f_{exp}$). However, the available data did not allow a detailed divertor power balance analysis. Questions remained as to whether the detachment was an inherent consequence of the SF formation, and how $q_{\|}$ was affected by the increased divertor $P_{rad}$ and $L_{\|}$. In spite of the formation of the highly-radiating detached SF region in NSTX, high core confinement was maintained for a full duration of the SF phase 500-600 ms (i.e. up to $10 \times \tau_E$). The peak heat flux reduction in the SF configuration (without gas seeding) was similar to that measured in the radiative divertor experiments conducted using $D_2$ or $CD_4$ seeding at $P_{SOL} \sim 3$ MW in the standard divertor configuration. Additional $CD_4$ or $D_2$ seeding during the SF phase using a divertor gas injector showed excellent divertor gas screening from the core, increased divertor radiation, and stable MARFE-free operation (unaffected confinement) [16, 17]. In the $CD_4$-seeded SF divertor, the divertor C III and C IV brightness profiles showed increased radiation, both in the intensity (i.e. due to the dependence of the carbon radiative cooling rate $L_C$ on $n_e, T_e$), and in the spatial extent, due to the SF divertor high-flux expansion zone [16].

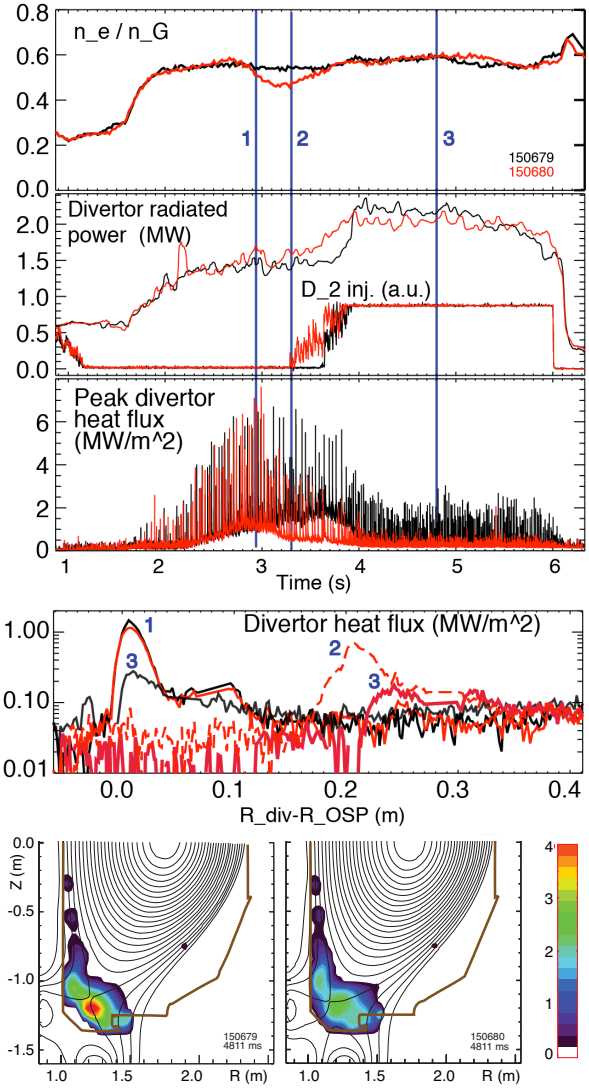


***Figure 3:*** *Comparison of DIII-D H-mode discharges with the standard (black traces) and SF-minus (red traces) configurations with $D_2$ puffing. Top panel: Time traces. Middle panel: divertor profiles measured in both discharges at 2.8 s (Label 1), 3.3 s (Label 2), and 4.8 s (Label 3). Bottom panel: divertor radiated power distribution at 4.8 s in the standard divertor discharge (left) and SF discharge (right).*

Density control and detachment with the SF divertor were further investigated in the initial SF experiments in DIII-D [7]. A lower divertor cryo-pump was used for particle removal, and gas puffing was used for steady-state density control in the range $(0.40 - 0.75) \times n_e/n_G$. Particle balance and neutrals analysis with the SF divertor are deferred to a future presentation, however, we note that density control was possible with the SF configuration. The cryo-pump entrance in both the standard and the SF discharges was located in the far-SOL, where neutral pressure and divertor $T_e$ were similar.

Radiative divertor and a partial OSP detachment in DIII-D are accessed by increasing the upstream density via gas puffing [18]. The SF divertor, albeit with a significant heat flux reduction, remained attached in 5 MW NBI heated H-mode discharges at lower densities ($n_e/n_G \sim 0.4 - 0.55$). At higher densities ($n_e/n_G \sim 0.55 - 0.75$), a partial OSP detachment was observed in both discharges with the standard and the SF configurations. The partial detachment was

accompanied by some confinement degradation (e.g., the H89L factor was reduced by 10-15 % cf. the lower density discharge shown in Figure 2). Time traces of two discharges with gas puffing are shown in Figure 3. The SF-minus configuration was formed at 3.0-3.2 s. Divertor heat flux profiles are compared at three times - before gas puffing (Label 1, both standard divertor), after SF formation and before gas puffing (Label 2, only the SF discharge), and during gas puffing (Label 3, standard vs SF-minus). As the SF-minus was formed, peak heat flux was reduced, mostly due to the increased plasma-wetted area (from $f_{exp}$ comparison), and then further reduced due to partial detachment. Peak heat flux was lower in the partially detached SF (cf. partially detached standard divertor). Tomographic reconstructions of divertor radiation showed that radiation was broadly distributed throughout the SF null zone, with occasional peaking in the null-point regions in higher density discharges. More importantly, despite an increase in $L_{\|}$ by 50-75 %, MARFE formation was not apparent in the SF configurations with gas seeding. In the partially-detached SF divertor at DIII-D peak divertor heat flux during ELMs was also significantly reduced (Figure 3).

**Summary** The emerging understanding of ELM and between-ELM divertor heat transport and radiation in the SF divertor from NSTX and DIII-D experiments provides support to the snowflake divertor configuration as a promising concept for divertor heat flux mitigation in future magnetic fusion devices. Near-future experiments are planned at DIII-D to study magnetic feedback control, pedestal evolution and parallel heat flux distribution in the SF configurations. The SF divertor is also being considered as a leading candidate for heat flux mitigation in the NSTX Upgrade tokamak presently under construction at Princeton Plasma Physics Laboratory [14, 17].

Supported by the US Department of Energy under Contracts DE-AC52-07NA27344, DE-AC02-09CH11466, DE-FC02-04ER54698, DE-FG02-08ER54989. The data shown in figures is from the DIII-D tokamak.

## References

[1] RYUTOV, D., Phys. Plasmas **14** (2007) 064502.
[2] PIRAS, F. et al., Phys. Rev. Lett. **105** (2010) 155003.
[3] CODA, S., Nucl. Fusion **51** (2011) 094017.
[4] SOUKHANOVSKII, V. et al., Nucl. Fusion **51** (2011) 012001.
[5] SOUKHANOVSKII, V. A. et al., Phys. Plasmas **19** (2012) 082504.
[6] SOUKHANOVSKII, V. A. et al., J. Nucl. Mater. **438S** (2013).
[7] ALLEN, S. L. et al., Initial snowflake divertor physics studies on DIII-D, in *Proc. 24th IAEA FEC - IAEA CN-197, San Diego, 8-13 October 2012*, Paper PD/1-2, Slides available at https://fec2012.iaea.org/.
[8] RYUTOV, D. et al., Phys. Plasmas **15** (2008) 092501.
[9] RYUTOV, D. et al., Plasma Phys. Control. Fusion **52** (2010) 105001.
[10] RYUTOV, D. D., Contrib. Plasma Phys. **52** (2012) 539.
[11] RYUTOV, D. D. et al., Plasma Phys. Control. Fusion **54** (2012) 124050.
[12] RYUTOV, D. et al., in *Proc. 24th IAEA FEC, San Diego, 2012*, Paper TH/P4-18.
[13] MAKOWSKI, M. A. et al., Phys. Plasmas **19** (2012) 056122.
[14] MENARD, J. et al., Nucl. Fusion **52** (2012) 083015.
[15] SOUKHANOVSKII, V. et al., Phys. Plasmas **16** (2009) 022501.
[16] SOUKHANOVSKII, V. A. et al., in *Proc. 39th EPS Conf. on Plasma Phys.*, page P5.049, Stockholm, Sweden, 2012.
[17] SOUKHANOVSKII, V. A. et al., in *Proc. 24th IAEA FEC, San Diego, 2012*, Paper EX/P5-21.
[18] PETRIE, T. et al., Nuc. Fusion **37** (1997) 643.